ACS OMEGA

Open Access

http://pubs.acs.org/journal/acsodf

Article

Assessing the Interaction between Dodecylphosphocholine and Dodecylmaltoside Mixed Micelles as Drug Carriers with Lipid Membrane: A Coarse-Grained Molecular Dynamics Simulation

Atefeh Gholizadeh, Sepideh Amjad-Iranagh,* and Rouein Halladj*

Cite This: *ACS Omega* 2024, 9, 40433−40445

Read Online

ACCESS | Metrics & More | Article Recommendations | Supporting Information

ABSTRACT: Integrating drugs into cellular membranes efficiently is a significant challenge in drug delivery systems. This study aimed to overcome these barriers by utilizing mixed micelles to enhance drug incorporation into cell membranes. We employed coarse-grained molecular dynamics (MD) simulations to investigate the stability and efficacy of micelles composed of dodecylphosphocholine (DPC), a zwitterionic surfactant, and dodecylmaltoside (DDM), a nonionic surfactant, at various mixing ratios. Additionally, we examined the incorporation of a mutated form of Indolicidin (IND) (CP10A), an anti-HIV peptide, into these micelles. This study provides valuable insights for the development of more effective drug delivery systems by optimizing the mixing ratios of DPC and DDM. By balancing stability and penetration efficiency, these mixed micelles can improve the delivery of drugs that face challenges crossing lipid membranes. Such advancements can enhance the efficacy of treatments for various conditions, including viral infections and cancer, by ensuring that therapeutic agents reach their intended cellular targets more effectively.

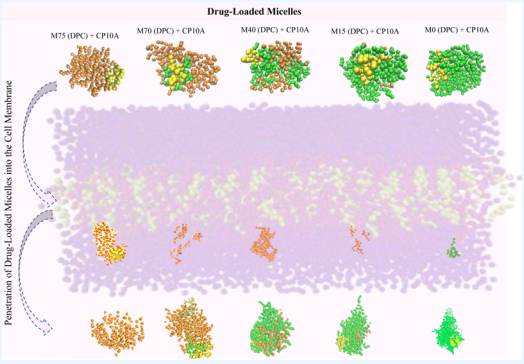

1. INTRODUCTION

The advent of nanotechnology in biological systems has significantly advanced the development of drug delivery systems.[1−4] Among the various nanoparticles, nanomicelles have emerged as particularly effective drug carriers.[5,6] These carriers are formed using amphipathic biomolecules, which possess both hydrophilic and hydrophobic properties, allowing for diverse structures and high drug-loading capabilities. Additionally, nanomicelles exhibit strong diffusivity into cell membranes, making them highly effective. The self-assembly of different amphiphilic molecules facilitates the design of new micelles with desirable features.[7,8]

Studies have shown that the stability, size, and shape of micelles in aqueous media are influenced by temperature.[9−12] Thus, understanding the structural properties of micelles is crucial for designing effective drug carriers. One challenge with drugs is their efficient diffusion through the cell membrane. Therefore, using a drug carrier compatible with the cell membrane is recommended.[13]

Dodecyl phosphocholine (DPC) is a zwitterionic surfactant with a polar phosphocholine head containing both negative and positive charges, making it a significant tool in studying lipid-associated proteins and peptides.[14−16] DPC has been used to enhance the permeability of drugs into membranes.[17] Dodecylmaltoside (DDM), a nonionic surfactant with a maltoside sugar headgroup, shares the same 12-carbon hydrocarbon chain as DPC but differs in chemical properties due to its headgroup.[18]

Earlier studies have primarily focused on using either pure DPC or DDM micelles as drug carriers.[19−21] In contrast, by optimizing the mixing ratios of DPC and DDM, we aim to develop drug delivery systems that balance stability and penetration efficiency. This study demonstrates an improvement in drug delivery efficiency by designing a mixed micelle using DPC and DDM surfactants.[19,,23]

This approach can improve the delivery of drugs that typically face challenges crossing lipid membranes. Such advancements have the potential to enhance treatments for various conditions, including viral infections and cancer, by ensuring that therapeutic agents reach their intended cellular targets more effectively.

Molecular dynamics (MD) simulations are invaluable for predicting particle movements and velocities in a system.[24−28] Coarse-grained molecular dynamics (CGMD) simulations provide a faster and more computationally efficient approach compared to atomistic simulations. By reducing atomic detail,

Received: March 15, 2024
Revised: August 30, 2024
Accepted: September 4, 2024
Published: September 16, 2024

CG simulations enable the study of large-scale processes and collective behaviors. However, CG simulations may sacrifice some atomic-level information, limiting the accuracy of certain interactions and structural features. Despite these challenges, recent advancements have shown that CG simulations can achieve results comparable to atomistic models in many cases.[29−32]

MD simulations have demonstrated that DPC micelles, due to their structural and functional similarity to lipid bilayers, serve as suitable models for membrane simulations.[15] A study comparing DPC and DDM micelles as protein carriers found that DPC micelles lose their regular orientation in nonaqueous media, while DDM micelles undergo fewer structural changes, providing better protection for proteins.[18]

Indolicidin (IND), an antimicrobial peptide (AMP) which is important to the human immune system, is the smallest known natural AMP, comprising of 13 amino acid residues (ILPWKWPWWPWRR-NH_2). Despite its small size, it is highly effective against microorganisms and HIV.[33] However, IND can be toxic to lymphocytes and erythrocytes.[34−36] To mitigate toxicity and enhance membrane permeability, scientists have introduced modifications to IND, resulting in a Pro to Ala mutant named CP10A (ILAWKWAWWAWRR-NH_2).[37−39]

Previous MD simulations and experimental studies on IND's interaction with lipid membranes have shown that IND predominantly binds with the hydrophilic region of the membranes.[37,40] Since both IND and CP10A are water-soluble, their translocation into the cell membrane is a complex process.[41]

MD simulations are highly effective for studying lipid membranes[42−44] and examining drug orientation and diffusion into cell membranes.[45−49]

In this study, we employed CG models of DDM and DPC to form both pure and mixed micelles, serving as carriers for CP10A within a mixed bilayer membrane composed of dipalmitoylphosphatidylcholine and cholesterol (DPPC/CHOL). DPPC was selected due to its significant presence in biological membranes.[50] Initially, we simulated the micelle structures under constant pressure (P = 1 bar) at three different temperatures: 298.15, 303.15, and 323.15 K. These temperatures were chosen to represent room temperature, a common biological system temperature (including the human body), and a physiological range for many biological systems, respectively.[51,52] We then calculated the structural properties of these micellar systems to determine the effects of temperature. Following this, we explored the interaction of CP10A with the micelles at room temperature (298.15 K).

2. SIMULATION METHODS

We utilized the GROMACS 2018.4 package[53,54] and the CG MARTINI force field V2.2[31] to conduct our MD simulations. Considering the significant presence of water in blood and its crucial role as a biological solvent, we employed the standard Martini model of water.[55]

In the standard Martini model of water, each bead represents a collection of four water molecules (AA model). While this CG representation has limitations, such as its inability to accurately capture water behavior near surfaces, it is important to note that water molecules exhibit high mobility and behave similarly in bulk water. Consequently, this approximation does not significantly affect the overall behavior of the system. Despite its potential deficits, the Martini model remains a reliable choice for studying water behavior in large-scale systems.[55]

For this research, we obtained the force field parameters for DPC, DDM, DPPC, and CHOL, as well as the all-atom structure of CP10A (PDB code 1HR1) from www.cgmartini.nl[31,56,57] and www.rscb.com,[37] respectively.

2.1. Initial Micelles. In this section, we used the PACKMOL program to generate five preassembled spherical micelles. PACKMOL helped us reduce the time required for the system to equilibrate. By using PACKMOL, we could fix the ratio of DPC to DDM in the micelles, ensuring consistency in composition across simulations. This enabled us to systematically investigate the impact of different mixing ratios on micelle stability[58] (Figure S1).

Initially, these preassembled micelles were placed within cubic boxes, which were then filled with water. The surfactant concentrations within the simulation boxes were set above their respective critical micelle concentration (CMC) values. For DPC and DDM, the CMC values are reported as 0.95 and 0.18 mM, respectively.[14,59]

To ensure system stability, energy minimization was performed using the steepest descent algorithm.[60] Following this, two 30 ns equilibration phase was conducted with controlled temperature and pressure (NVT and NPT ensembles). Temperature control utilized the v-rescale method,[61] and pressure control employed the Berendsen coupling method,[62] with relaxation times of τ_T = 1.0 ps and τ_P = 5.0 ps, respectively.

After equilibration, MD simulations were run for 300 ns with periodic boundary conditions. These simulations were conducted at a constant pressure of 1 bar and at three temperatures: 298.15, 303.15, and 323.15 K. Temperature control during the MD simulations continued to use the v-rescale method, while pressure control switched to the Parrinello−Rahman coupling method,[63,64] with relaxation times of τ_T = 1.0 ps and τ_P = 12.0 ps, respectively. For nonbonded interactions, a short-range electrostatic cutoff of 1.1 nm was applied, along with a short-range van der Waals cutoff of 1.1 nm for bonded interactions.

The optimal time step for CGMD simulations is reported to be approximately 20−40 fs.[65,66] In this study, a time step of 25 fs was used, with the neighbor list updated every 20th step. Details regarding the simulation box characteristics are provided in Table 1.

Table 1. Simulation Parameters for Initial Micelles

	number of molecules in simulation box				
system	water	DPC	DDM	simulation box size (nm^3)	simulation time (ns)
M75	10,077	75	0	11 × 11 × 11	300
M70	10,266	70	5	11 × 11 × 11	300
M40	10,080	40	35	11 × 11 × 11	300
M15	10,180	15	60	11 × 11 × 11	300
M0	10,405	0	75	11 × 11 × 11	300

2.2. Drug and Micelles Interaction. In this section, the Martinize tool,[31,67] a Python script, was used to generate a CG model of CP10A from its atomistic representation. Figure S2 illustrates the atomistic (AA) and coarse-grained (CG) models of CP10A, visualized using VMD software.[68]

https://doi.org/10.1021/acsomega.4c02551
ACS Omega 2024, 9, 40433−40445

Table 2. Simulation Parameters for Micelles and Drug

system	number of molecules in simulation box					simulation box size (nm^3)	simulation time (ns)
	water	DPC	DDM	CP10A	ions (CL)		
M75/CP10A	10,292	75	0	1	3	11 × 11 × 11	300
M70/CP10A	10,246	70	5	1	3	11 × 11 × 11	300
M40/CP10A	10,150	40	35	1	3	11 × 11 × 11	300
M15/CP10A	10,094	15	60	1	3	11 × 11 × 11	300
M0/CP10A	11,618	0	75	1	3	11 × 11 × 11	300

The micelles obtained from Section 2.1, along with the CG model of CP10A, were randomly placed within the simulation box to investigate the interactions between the micelles and CP10A. To neutralize the net charge of CP10A, solvent molecules and Cl^- ions were added. The energy minimization and equilibration procedures described in Section 2.1 were also applied to this system. To simulate an in vitro situation at room temperature, a reference temperature of 298.15 K was selected for the subsequent MD simulations. The specifications of the simulation boxes are outlined in Table 2.

2.3. Membrane Interaction with Micelles and Drug. To obtain a mixed bilayer, we utilized the Python script insane.py[57] to create a membrane structure under near-equilibrium conditions. Using insane.py, we constructed a 4:3 mol ratio of DPPC/CHOL mixed-bilayer, consisting of 386 DPPC molecules and 289 CHOL molecules per leaflet, within a simulation box measuring 20 × 20 × 10 nm^3. MD simulations were performed for a duration of 300 ns at a temperature of 298.15 K and a pressure of 1 bar. Previous studies[69] have reported a lower gel−fluid phase transition temperature for DPPC/CHOL membranes compared to pure DPPC membranes, hence the simulation was conducted at room temperature (298.15 K).

To study the permeation process of different systems into the membrane, we utilized potential of mean force (PMF) calculations using umbrella sampling. This method provides valuable insights into the energetics and thermodynamics of the interaction between drug carriers and the lipid bilayer membrane.[70] In our simulation setup, the drug carriers were initially placed in bulk water, starting at a distance of 5.0 nm from the membrane. The entire system was contained within a simulation box measuring 19 × 19 × 35 nm^3. To facilitate the pulling process, the carriers were restrained in the x and y directions and pulled across the lipid bilayer along the reaction coordinate (z-axis). A harmonic spring potential with a force constant of 1000 kJ/mol·nm^2 and a constant velocity of 0.002 nm/ps was employed to ensure a smooth and controlled pulling process.[71]

For each simulation box, we extracted a set of configurations where the displacement of the micelles' center of mass (CoM) along the z-direction was 0.2 nm. To ensure equilibration, each configuration underwent a preliminary equilibration phase followed by a 10 ns production run. During these stages, a biasing harmonic potential with a force constant of 1000 kJ/mol·nm^2 was employed to guide the carriers across the membrane. The PMF was then calculated using the weighted histogram analysis method (WHAM).[72] WHAM is a powerful technique that allows for the estimation of the PMF by combining data from multiple simulations and generating a probability distribution function (PDF). This approach enables the construction of a histogram, providing insights into the probability of observing distinct states along the reaction coordinate.

By employing umbrella sampling and subsequent PMF calculations using WHAM, we obtained valuable information regarding the energy profile of the drug carriers' permeation process through the lipid bilayer membrane. These insights contribute to a better understanding of the interactions involved and can guide the design of optimized drug delivery systems.

3. DATA ANALYSIS METHODS

In this section, we will discuss the methods and analyses we used to reach our results. The theories and explanations for each analysis are provided in detail. In the next section, the results will be discussed.

3.1. Initial Micelles. To investigate the impact of temperature on the stability and structural properties of micelles, we calculated various parameters, including the radius of gyration (R_g), moments of inertia (I), asymmetry parameter (α), RDf, and solvent accessible surface area (SASA) at three different temperatures.

The R_g provides insights into the size and equilibration state of the micelle systems. We calculated R_g using the GROMACS *gmx gyrate* tool.[54,73]

The shapes of micelles were determined by computing the I. The micelle's α is defined as $\alpha = (2I_1 - I_2 - I_3)/(I_1 + I_2 + I_3)$.[15] This parameter quantifies the extent to which the micelle's structure deviates from perfect symmetry, providing a measure of its asymmetry and capturing any irregularities or imbalances in its shape or component distribution. For perfectly spherical structures, the α value is 0.[74]

The SASA is a key parameter for understanding the interfacial properties and compactness of micelles. It measures the portion of the micelle's surface that is accessible to solvent molecules, specifically water in this case.[75] We calculated SASA using the GROMACS *gmx sasa* tool.[54]

To examine the interior properties of the micelles and assess the probability distribution of water molecules around the micelle's CoM, we used the GROMACS *gmx rdf* tool.[54]

3.2. Drug and Micelles Interaction. The stability of drug-loaded micelles can be evaluated using Root Mean Square Deviation (RMSD) by examining changes in the micelle's shape, size, and alterations in the drug's secondary structure. These changes occur due to interactions with other molecules within the simulation box, with the initial frame serving as the reference state for comparisons.

We utilized the *gmx rmsd* tool[54] to assess the stability of micelle-drug interactions. This tool monitors positional changes throughout the simulation, comparing them to the initial frame to determine stability.

Additionally, the *gmx mindist* tool[54] was employed to calculate the minimum distances between the CoM of the selected groups (the micelle and the drug), allowing us to determine their contact number during the simulation.

https://doi.org/10.1021/acsomega.4c02551
ACS Omega 2024, 9, 40433−40445

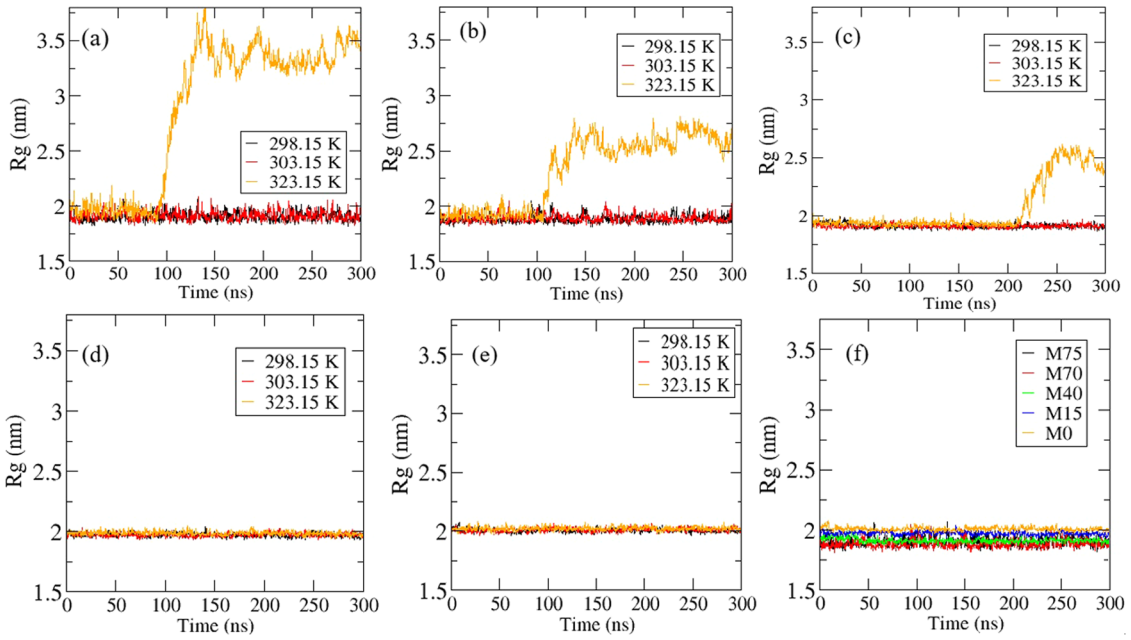

Figure 1. Comparison of R_g at Different Temperatures over a 300 ns simulation. The figure represents the variation in the R_g among different micelle systems at different temperatures. Micelles M75, M70, M40, M15, and M0 are represented in panels (a−e), respectively. Panel (f) presents a comparison of the radius of gyration for these five systems specifically at a temperature of 298.15 K.

The Gibbs free energy of solvation, ΔG (kJ/mol), is a significant property that can be estimated using the well-known equation[76]

$$\Delta G = \Delta H - T\Delta S \tag{1}$$

A substance spontaneously dissolves in water if the overall Gibbs free energy of the solution is negative, indicating an energetically favorable process.[76] In this study, we used the GROMACS *gmx sasa* tool to estimate the free energy of solvation, based on changes in the solvent-accessible surface area.[77]

3.3. Membrane. For a membrane composed of a single type of lipid, the area per lipid (APL) is calculated by first determining the membrane's surface area, then dividing it by the number of lipids in one leaflet. However, in a mixed membrane that includes CHOL, the method for calculating APL differs and can be executed using the following equation[78]

$$A_{\mathrm{DPPC}} = \frac{2A}{N_{\mathrm{DPPC}}}\left(1 - \frac{N_{\mathrm{CHOL}}V_{\mathrm{CHOL}}}{V - N_{\mathrm{W}}V_{\mathrm{W}}}\right) \tag{2}$$

In this equation, N_{W}, N_{CHOL} and N_{DPPC} present the number of water molecules, CHOL molecules, and DPPC molecules, respectively. A and A_{DPPC} denote the area of the simulation box and the area per lipid. V, V_{W}, and V_{CHOL} stand for the volume of the simulation box, the volume of water molecules in the box, and the volumes of CHOL molecules in the simulation box, respectively. This equation is derived from the following equations[78]

$$A_{\mathrm{DPPC}} = \frac{2V_{\mathrm{DPPC}}}{h} \tag{3}$$

where h represents the average thickness of the bilayer, and V_{DPPC} denotes the volume of a single DPPC molecule. The values of h and V_{DPPC} can be calculated as follows

$$h = \frac{V - N_{\mathrm{W}}V_{\mathrm{W}}}{A} \tag{4}$$

and

$$V_{\mathrm{DPPC}} = \frac{V - N_{\mathrm{W}}V_{\mathrm{W}} - N_{\mathrm{CHOL}}V_{\mathrm{CHOL}}}{N_{\mathrm{DPPC}}} \tag{5}$$

3.4. Membrane Interaction with Micelles and Drug. To determine the self-diffusion coefficient, the mean square displacements (MSDs)[53] of the drug molecule and micelles were analyzed over the last 2 ns. The MSD measures the displacement of beads from their initial positions over a defined time period. The following equation is used to calculate the MSD[54]

$$\mathrm{MSD} \equiv \langle |x(t) - x_0|^2 \rangle = \frac{1}{N}\sum_{i=1}^{N} |x^i(t) - x^i(0)|^2 \tag{6}$$

where N stands for a number of particles, x_0 refers to the initial position of the particle, and $x(t)$ shows particle displacement in a defined time period. To calculate self-diffusion coefficients, we obtained the linear slope of the MSD plot using the Einstein relation.[79]

$$D = \frac{1}{6}\lim_{n\to\infty}\left(\frac{\mathrm{dMSD}}{\mathrm{d}t}\right) \tag{7}$$

Interactions between the membrane and drug/micelle can be expressed in terms of binding energy.[80] There are various methods for calculating free energy, among which one of the most effective is computing the PMF using umbrella sampling (US).[80] Determining the PMF is crucial for specifying the optimal position of the drug within membranes.[72] To achieve this, we used WHAM.[54]

4. RESULTS AND DISCUSSION

4.1. Initial Micelles. The R_g offers valuable information about the size and equilibration state of the micelle systems.

https://doi.org/10.1021/acsomega.4c02551
ACS Omega 2024, 9, 40433−40445

Table 3. Comparison of Micelle Properties Before and After Drug Loading and the Influence of Temperature[a]

		before drug loading					
system	temperature (K)	R_g (nm)	SASA (nm^2)	I_1[b]	I_2[b]	I_3[b]	α
M75	298.15	1.903	147.039	7.8199	6.9941	4.7641	0.198
	303.15	1.914	148.509	7.9314	7.1472	4.7191	0.201
	323.15	2.872	154.775	21.2962	19.3842	6.2161	0.362
M70	298.15	1.885	147.972	7.6681	7.1472	5.1694	0.164
	303.15	1.889	149.368	7.7075	6.9409	5.1870	0.165
	323.15	2.330	155.774	13.0160	11.4966	6.2045	0.271
M40	298.15	1.912	162.837	8.5951	7.9253	7.1176	0.090
	303.15	1.910	163.670	8.5566	7.8852	7.1505	0.088
	323.15	2.067	170.537	10.6663	9.9180	7.3649	0.144
M15	298.15	1.971	171.563	10.1604	9.3633	8.5367	0.078
	303.15	1.972	178.874	10.1418	9.3886	8.5520	0.083
	323.15	1.985	185.256	10.3083	9.5275	8.6391	0.086
M0	298.15	2.007	187.034	11.1247	10.3167	9.4740	0.079
	303.15	2.011	188.786	11.1440	10.3922	9.5038	0.077
	323.15	2.022	195.113	11.2891	10.5092	9.6016	0.078
	after drug loading						
M75	298.15	1.910	158.8682	7.9046	7.0907	4.7347	0.201
M70	298.15	1.911	156.469	7.9577	7.2002	5.1347	0.176
M40	298.15	1.956	170.115	8.6849	8.0090	7.2127	0.089
M15	298.15	1.985	184.854	10.2411	9.5528	8.6745	0.079
M0	298.15	2.018	193.388	11.2650	10.4701	9.5457	0.080

[a]Simulations were conducted at three different temperatures to assess the temperature effect on micelle properties. Drug loading was exclusively performed at 298.15 K, and the properties of the micelles are reported at this temperature. [b]I in (10^4 amu·nm^2).

Figure 1 illustrates the variations in R_g for different micelles at the three temperatures.

As depicted in Figure 1(a), the R_g for the M75 micelle shows the highest fluctuation at 323.15 K, reaching approximately 3.5 nm after 150 ns. This significant increase in R_g suggests instability in the micelle structure. However, with a higher concentration of DDM within the micelle, the system becomes more temperature-resistant, resulting in reduced fluctuations in R_g at 323.15 K. This reduced fluctuation is evident in both the M15 and M0 micelles, as shown in Figure 1. Additionally, Figure 1(f) demonstrates that all systems exhibit stability at 298.15 K.

These findings indicate that between two surafctant that we studied, DDM is the most stable micelle at higher temperatures. However, further analysis is necessary to draw a comprehensive conclusion regarding the suitability of DDM and DPC micelles as drug carriers, which will be addressed in subsequent sections. Notably, the calculated values of the R_g for the DPC and DDM micelles in this study are consistent with those reported in previous atomistic studies.[15,81,82] Detailed R_g values for different systems can be found in Table 3.

These observations underscore the importance of DDM concentration as a nonionic surfactant in maintaining micelle stability under varying temperature conditions. While the M75 micelle demonstrates significant instability at elevated temperatures, the addition of DDM appears to mitigate these effects, leading to a more stable configuration. This stability is crucial for the effective delivery of drugs, as it ensures that the micelle maintains its integrity and interaction properties throughout the delivery process.

The average values of the I and the α for the micelles over a 300 ns simulation are reported in Table 3. As observed, the α value increases at higher temperatures, particularly for the M75 micelle, with a value of 0.198 at 298.15 K and 0.362 at 323.15 K. Changes in the α at higher temperatures may result from alterations in the micelle's molecular arrangement or conformation. These changes can lead to a prolate shaped structures, making the micelle more exposed to water.[74]

The reported α values for M75 and M0 in Table 3 are consistent with previous atomistic studies of DPC[15,81] and DDM micelles.[82]

The solvent-accessible surface area (SASA) value reflects the extent of contact between the micelle and its surrounding solvent environment. It considers both the hydrophilic head groups, which are exposed to water, and the hydrophobic tails within the micelle core. A higher SASA value indicates a larger exposed surface area and greater interaction between the micelle and solvent molecules. This increased exposure can lead to greater susceptibility to solvent-mediated effects and potential destabilization of the micelle structure. Conversely, a lower SASA value suggests a more compact micelle structure with less exposure of the hydrophobic tails to the surrounding water molecules. This compactness indicates a less hydrated micelle structure and tighter packing arrangement of surfactant molecules within the micelle core, resulting in reduced access for solvent molecules.[83,84] Table 3 also compares these parameters before and after drug loading. The data indicate an increase in the micellar radius following drug incorporation, suggesting structural changes due to the presence of the drug.

Figure 2 demonstrates the variations observed in the radial distribution function (RDFs) of water among the studied systems at 298.15 K.

Analysis of the RDFs from CoM of micelles reveals that the RDF of water for M0 exhibits a minimum at a distance of 1.25 nm, whereas for M75, the minimum is observed at 0.9 nm. This minimum indicates the distance at which water molecules are most likely to be found around the micelle. It is reasonable to infer that a larger distance to the minimum in the RDF plot for M0 suggests a relatively larger hydrophobic core compared

https://doi.org/10.1021/acsomega.4c02551
ACS Omega 2024, 9, 40433−40445

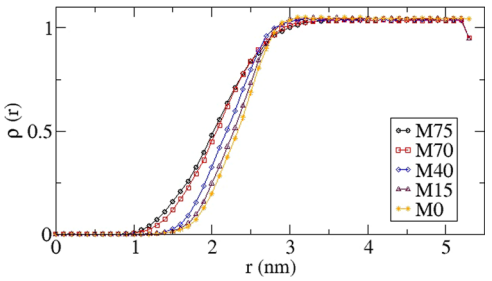

Figure 2. Radial density profile of water in five different systems at a temperature of 298.15 K. Here, r denotes the distance from the CoM of the micelle.

to M75.[85] A larger hydrophobic core generally corresponds to a larger surface area and potentially a less compact micelle structure, allowing for increased interaction with solvent molecules.[85]

These observations highlight the critical role of micellar composition and structure in determining their stability and interaction with the surrounding solvent. The increase in the α at higher temperatures for the M75 micelle indicates a significant conformational change, making the micelle more susceptible to interaction with water molecules. This is further supported by the SASA values, where higher SASA indicates greater exposure to the solvent and potential destabilization risks. The RDFs provide additional insights, showing how water molecules interact with different micelles, with M0 having a larger hydrophobic core, thus offering a different interaction dynamic compared to M75.

Comparing our results with previous studies, we found that the properties of M75 and M0 align with those reported in earlier researches.[15,81,82]

4.2. Drug and Micelles Interaction. To evaluate the structural stability and interactions of drug-loaded micelles, we conducted an RMSD analysis from CoM of micelle over the course of 300 ns simulations at 298.15 K.

Figure 3(a) presents the results of the RMSD analysis for five micellar systems. In this analysis, systems with lower RMSD fluctuations are typically considered more structurally stable than systems with larger RMSD fluctuations. This is because less variation in RMSD values indicates fewer changes in the system's structure over the course of the simulation, suggesting that it is maintaining its initial conformation more consistently. The RMSD plot for the M75/CP10A system shows significant fluctuations, indicating instability and weak interactions between M75 and CP10A. However, as the DDM concentration within the micelles increases, the fluctuations diminish, and the RMSD exhibits lower values, signifying greater stability. In Figure 3(b), the distances between the CoMs of the micelle and the drug are shown, highlighting moments when this distance reaches its minimum (less than 0.6 nm). The M75/CP10A system exhibits the most fluctuation, reaching the minimum distance after 100 ns, suggesting that M75 and CP10A may undergo significant structural changes. As the simulation progresses, reduced fluctuations and stabilization indicate that the system is moving toward equilibrium. Additionally, as the DDM concentration in the micelles increases, fluctuations diminish faster. In contrast, the M0/CP10A group shows a minimum distance at t = 0 ns, indicating a strong initial interaction or affinity between the micelle and the drug.[54]

Figure 3(c) illustrates the number of contacts between the micelle and the drug when the distance between their respective CoMs is 0.6 nm. For the M75/CP10A system, the number of contacts is zero at the beginning of the simulation, suggesting no initial interaction. In contrast, the M0/CP10A system shows a larger number of contacts from the start, suggesting a strong initial interaction between the micelle and the drug.[54]

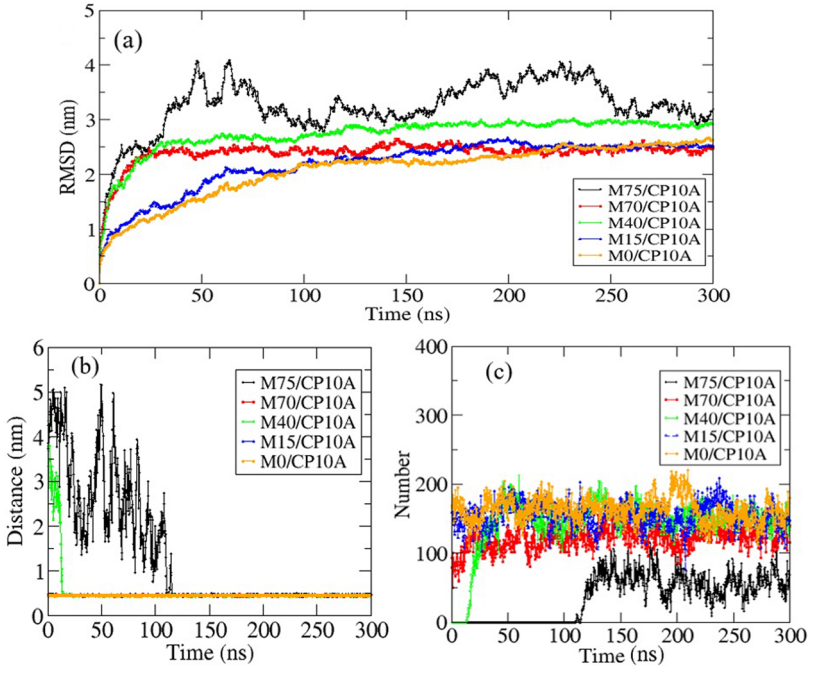

Figure 3. (a) Structural drift, as measured by RMSD from the initial structure, against time for five micellar systems at 298.15 K, over a 300 ns simulation. (b) The figure shows the distances between the CoM of the micelles and CP10A. (c) The number of contacts between micelles and CP10A where their CoM distances from each other are less than 0.6 nm.

https://doi.org/10.1021/acsomega.4c02551
ACS Omega 2024, 9, 40433−40445

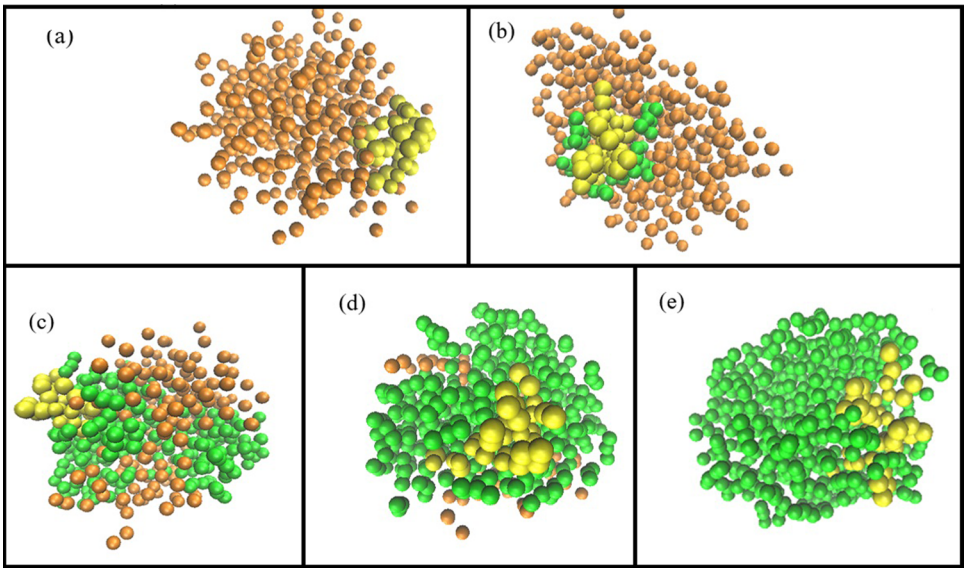

Figure 4. Interactions of CP10A with (a) M75, (b) M70, (c) M40, (d) M15, and (e) M0, as well as the depth of CP10A's diffusion into these micelles at 298.15 K. Orange: DPC. Yellow: CP10A. Green: DDM.

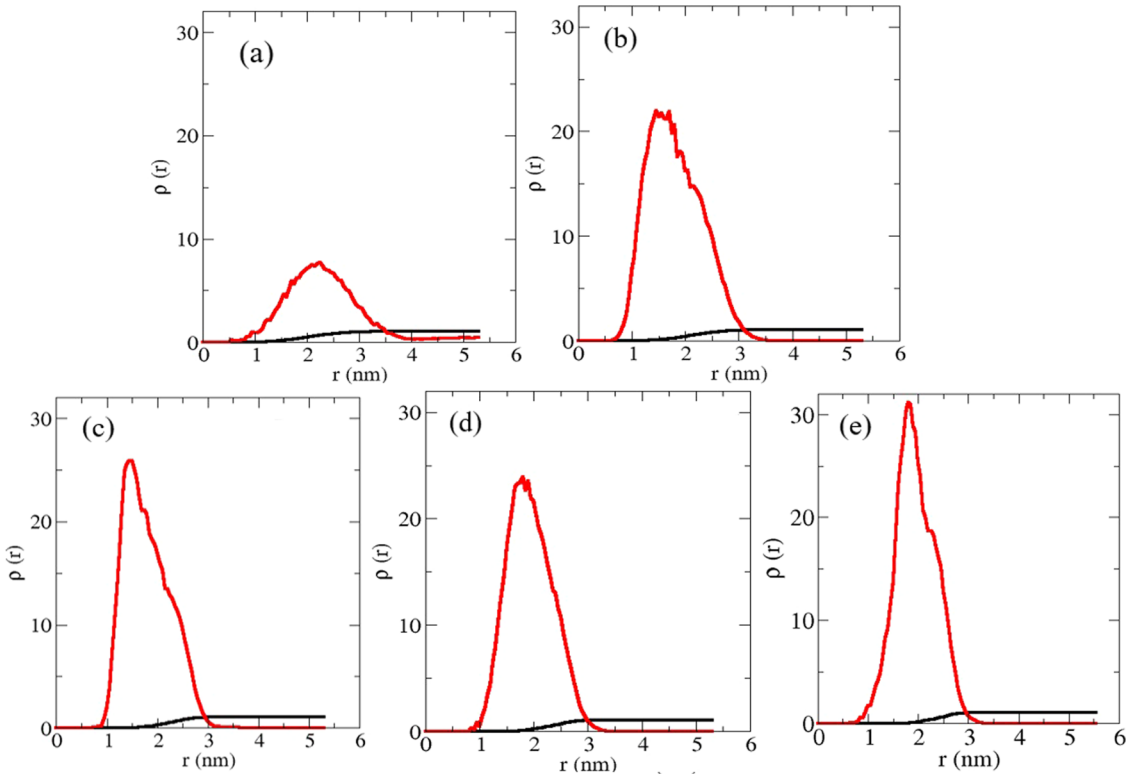

Figure 5. RDF ($\rho(r)$) of water (depicted in black) and CP10A (depicted in red) for each system, calculated from the CoM of the micelles, at 298.15 K. (a) M75. (b) M70. (c) M40. (d) M15. (e) M0.

These observations highlight the differing interaction dynamics between the systems. The M75/CP10A system requires time to establish interactions, which might suggest initial structural incompatibility or the need for structural reorganization. Conversely, the M0/CP10A system demonstrates an immediate affinity, indicating a more stable and compatible interaction from the onset. This analysis underscores the importance of micellar composition in determining the efficiency and stability of drug-micelle interactions.

Figure 4 demonstrates the extent to which CP10A is embedded within the micelles and its stronger affinity for binding with DDM molecules compared to DPC molecules. These simulation snapshots corroborate the previous RMSD analysis, confirming that CP10A and M0 are more likely to form bonds with each other, whereas CP10A and M75 exhibit weaker interactions, as seen in Figure 4(a).

Additionally, the RDFs of water and CP10A, calculated from the CoM of the micelles at 298.15 K, were used to determine the location of the loaded drug and surrounding water

https://doi.org/10.1021/acsomega.4c02551
ACS Omega 2024, 9, 40433−40445

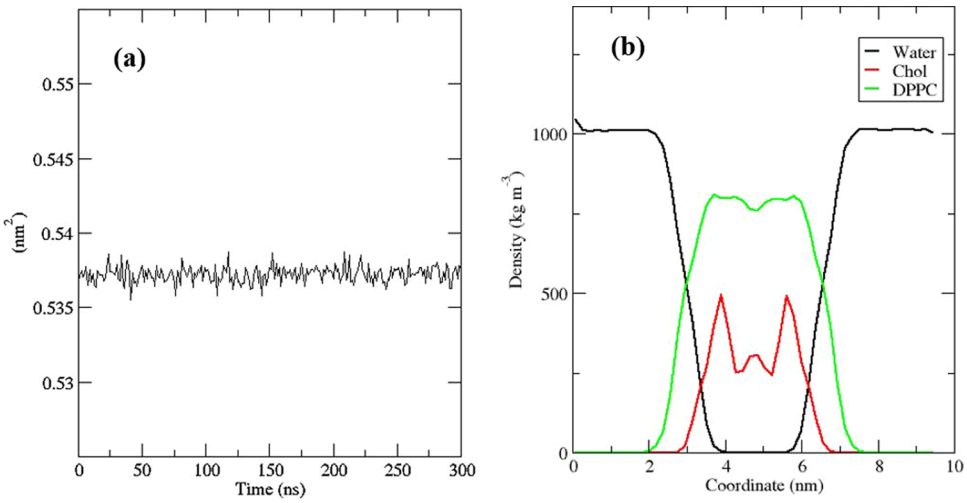

Figure 6. (a) APL of a mixed DPPC bilayer with 40% CHOL over a 300 ns simulation, (b) mass density.

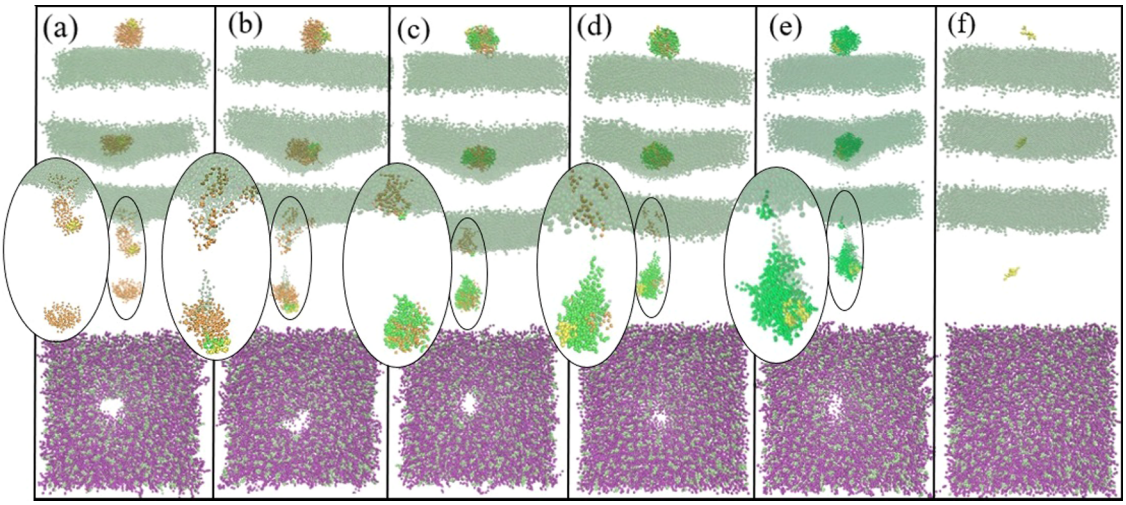

Figure 7. Above: (side view) in each panel the snapshots were taken at various stages of the simulation during 8 ns at 298.15 K to indicate the best view of the interaction between the membrane and micelles, while either micelles or drugs are gradually drawn through the membrane. Below: (top view) the effect of diffusion process into the membrane perturbation. (a) M75. (b) M70. (c) M40. (d) M15. (e) M0. (f) CP10A.

molecules. The RDF plots in Figure 5 indicate that CP10A tends to bind at the water/surfactant interface rather than diffusing into the interior of the micelles. Across all systems, CP10A shows a higher probability of interacting with micelles composed of DDM molecules. Furthermore, this analysis reveals that the RDF of water remains consistent with Figure 2, suggesting that drug loading does not affect water penetration into the micelles.

Figure 5(a) shows that the RDF ($\rho(r)$) peak intensity for CP10A is approximately 8 at a distance of 2.1 nm from the micelle CoM. This $\rho(r)$ intensity increases with a higher percentage of DDM in the micelles. Figure 5(b−e) indicate that for M70, M45, M15, and M0, the $\rho(r)$ intensity for CP10A is about 22 at a distance of 1.9 nm from the micelle CoM, 25 at a distance of 1.9 nm, 25 at a distance of 1.9 nm, and 32 at a distance of 1.9 nm, respectively.

The interaction of CP10A with micelles and the extent of its embedment are comparable to the findings in the previous study on DDM and DPC micelle interactions with peptides.[86]

The derived values of ΔG for CP10A, M75, M70, M40, M15, and M0 are 62.889, 773.067, 759.334, 671.882, 608.445, and 571.267 (kJ/mol), respectively. Higher free energy of solvation values suggest a stronger tendency for DPC and DDM molecules to aggregate and form micelles rather than to dissolve in water. A comparative analysis between M75 and M0 reveals that ΔG for M75 is greater than M0. This implies that DPC molecules have a higher propensity to interact with each other, leading to the formation of compact micelles. On the other hand, CP10A, with its lower ΔG value, is more hydrophilic compared to DPC and DDM. This indicates that, as a drug, it may encounter more difficulty in permeating through the membrane. However, as observed in the previous sections, CP10A exhibits a strong affinity toward DDM molecules, which could have potential implications in its membrane permeability and interaction dynamics. Furthermore, the contributions of enthalpy (ΔH) and entropy ($T\Delta S$) to the overall Gibbs free energy provide additional insights into the solvation process. Changes in enthalpy reflect the strength of molecular interactions such as hydrogen bonding and van der Waals forces, while entropy changes indicate the degree of disorder or molecular freedom in the system.

4.3. Membrane. The properties of the simulated membrane were assessed by calculating the RDF of water and the APL. These calculated values are displayed in Figure 6.

https://doi.org/10.1021/acsomega.4c02551
ACS Omega 2024, 9, 40433−40445

The APL is a vital parameter in lipid simulation studies, used to examine the equilibrium state of a lipid membrane in the simulation box.

The APL for the simulated membrane in this study is depicted in Figure 6(a). The APL is approximately 0.537 nm^2, with minor fluctuations, indicating that the bilayer membrane is in an equilibrium state. Previous research has shown that the average APL for a pure DPPC membrane is around 0.63 nm^2 at 315.15 K.[78,87] However, mixed DPPC/CHOL bilayers typically exhibit a lower APL than pure DPPC membranes,[78,80] and temperature variations can also influence the APL.[88] In agreement with these findings, the APL of a DPPC bilayer containing 40% CHOL at 323 K was reported to be 0.542 nm^2.[78] Therefore, the consistency of our simulation results with previous research validates the accuracy of the CG simulation in this work at 298.15 K.

Figure 6(b) illustrates a decreasing trend in water density as the densities of DPPC and CHOL increase, suggesting that water molecules have not penetrated the hydrophobic core of the membrane.

4.4. Membrane Interaction with Micelles and Drug.

Figure 7 shows how micellar systems and the single drug molecule penetrate into the lipid membrane during 8 ns of pulling simulation at 298.15 K.

This figure illustrates the decomposition of M75, leading to the loss of its spherical structure due to diffusion, resulting in the increased attachment of DPC surfactants to the bilayer. Conversely, with the higher presence of DDM in the micelles, they exhibited enhanced stability and underwent minimal shape changes during the penetration process. As it can be seen in this figure, M75 failed to transport the drug, causing both the drug and a specific amount of DPC surfactants to adhere to the membrane. In contrast, M0 successfully traversed the membrane without altering its shape. For a more dynamic insight, animated images (GIFs) showcasing the simulation process and the observed changes throughout the study can be found in the Supporting Information.

To assess the self-diffusion coefficient, we analyzed the MSDs of both the drug molecule and micelles during the final 2 ns of the simulation, depicted in Figure 8.

At a temperature of 298.15 K, the calculated self-diffusion coefficients ($\times 10^{-6}$ $cm^2 \cdot s^{-1}$) for CP10A, M75, M70, M40, M15, and M0, derived from the MSD plots, are as follows: 1.5294, 1.2010, 1.0933, 1.0466, 1.0201, and 1.0144, respectively.

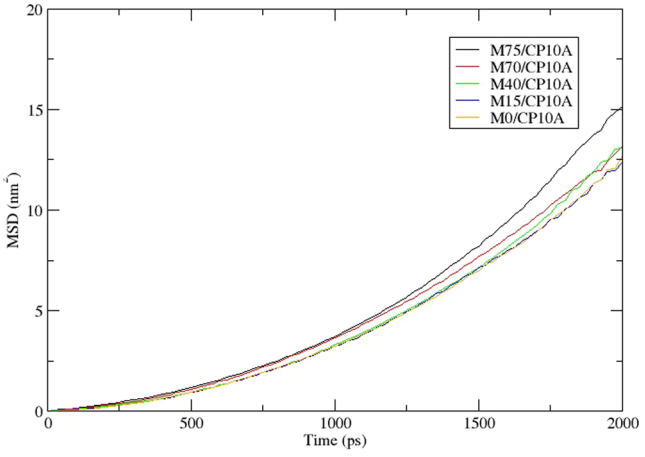

Figure 8. MSD of five simulated systems at 298.15 K.

Notably, among the micelles, M75 exhibits the highest self-diffusion coefficient at 1.2010×10^{-6} $cm^2 \cdot s^{-1}$, indicating its relatively swift movement compared to other micelles. As the DDM proportion within the micelles increases (transitioning from M75 to M0), the self-diffusion coefficients decrease. This trend suggests that micelles comprising a greater proportion of DDM molecules tend to have lower mobility, likely due to their enhanced stability and larger size, which can impede their movement. This decreased mobility can be attributed to several factors. First, micelles with higher DDM content have increased molecular weight, which inherently reduces their diffusion rates. Second, the stronger hydrophobic interactions in DDM-rich micelles result in more stable structures. These more stable structures are less likely to undergo conformational changes, which further limits their movement. Furthermore, the size and shape of the micelles play a role; larger and more spherical micelles, typical of those with higher DDM content, diffuse more slowly. Thus, the combination of increased molecular weight and enhanced hydrophobic interactions explains the observed relationship between micelle composition, stability, and mobility.

The process of micelle and drug diffusion into the membrane can be effectively elucidated through an analysis of binding energy. The results derived from WHAM method across all examined systems are visually represented in Figure 9.

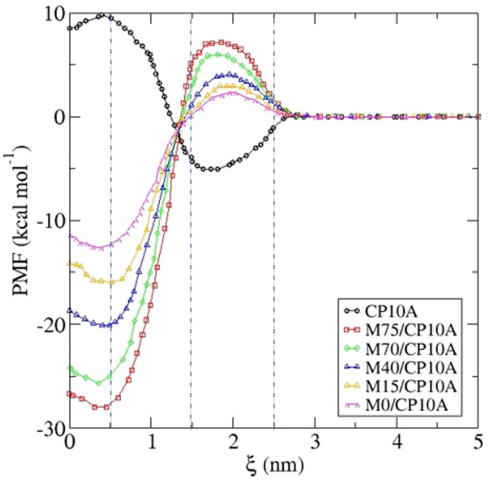

Figure 9. Energy profiles ($kcal \cdot mol^{-1}$) of all the systems across the membrane as a function of the normal distance to the bilayer midplane (ξ(nm)) at 298.15 K.

In this depiction, a striking aspect is the distinctive behavior exhibited by CP10A.

At a distance of 0.5 nm from the CoM of the membrane, representative of the spacing between the membrane's layers, the nonpolar attributes of this zone coupled with sparse water presence induce negligible fluctuations in the penetration rates of components within this locale.[89]

Within the range of 0.5−1.5 nm from the CoM of the membrane, the formidable density of the hydrophobic membrane region creates substantial resistance to the penetration of hydrophilic entities. In contrast, hydrophobic entities effortlessly permeate this sector, resulting in reduced energy profiles for micellar systems. Noteworthy is CP10A,

https://doi.org/10.1021/acsomega.4c02551
ACS Omega 2024, 9, 40433−40445

which exhibits the highest energy levels in this domain, symbolizing its hydrophilic nature. Conversely, minimal free energy is detected in the hydrophilic sections, denoting an optimized structural configuration within the DPPC/CHOL mixed membrane.

Moving from 1.5 to 2.5 nm, the escalating density of the membrane presents obstacles to the entry of external components due to interactions among the hydrophilic membrane components. Despite this hindrance, the interplay of membrane lipids does not deter the infiltration of hydrophilic structures into this realm.

Furthermore, in the zone spanning 2.5−5 nm from the CoM of the membrane, the combination of lower density in the hydrophobic segment along with heightened hydration levels results in characteristics reminiscent of the aqueous milieu. This gives rise to uniformly flat energy profiles across these systems.

Energy profiles of mixed micelles indicate that the peak energy level emerges notably between 1.5 and 2.5 nm, suggesting that their traversal through the hydrophilic membrane segment necessitates increased energy. M0 has the lowest peak in the energy profile during the penetration of the hydrophilic part. On the other hand, M75 encounters more difficulty penetrating this region.

The PMF plots for the studied systems in this work show results consistent with previous studies on the penetration of different molecules into the cell membrane. The peaks of the plots are comparable with those found in previous studies.[72,90,91]

The primary objective of this study was to identify the optimal mixing ratio for micelles to serve as effective drug carriers. Based on the PMF plot, among the five micellar systems analyzed, the most favorable choice for transporting drugs is a balanced blend of DDM and DPC. This particular micelle configuration demonstrates relatively lower energy requirements during its penetration into the membrane.

5. CONCLUSIONS

Previous studies have primarily focused on the use of either pure DPC or DDM micelles. This study demonstrates that the combination of DPC and DDM creates a robust carrier system for drug delivery, achieving a balance between stability and penetration efficiency. Our findings indicate that DDM exhibits greater stability during environmental changes, while DPC demonstrates enhanced membrane penetration. Consequently, a micelle comprising both DPC and DDM represents an optimal choice for a drug carrier. Among the studied micelles, the M40 micelle stands out as the most suitable option for drug delivery, showcasing the most effective diffusion into the lipid membrane. Additionally, this micelle exhibits notable resistance against deformation and significant energy reduction during membrane penetration, highlighting its stability and propensity to pass through the center of the membrane.

Future research should focus on translating these findings into clinical applications. This could involve exploring the in vivo behavior of these mixed micelles and their potential to enhance drug bioavailability and reduce side effects. Additionally, developing tailored micelle formulations for specific therapeutic agents could lead to more effective and personalized treatment options.

ASSOCIATED CONTENT

Supporting Information

The Supporting Information is available free of charge at https://pubs.acs.org/doi/10.1021/acsomega.4c02551.

Additional Information: Preassembled micelles were generated using the PACKMOL program. Comparative representation of all-atom and coarse-grained models of CP10A are shown in (Figures S1−S2); for a more dynamic insight, animated images (GIFs) showcasing the simulation process and the observed changes throughout the study can be found in (Animated Figures S1−S6) (PDF)

AUTHOR INFORMATION

Corresponding Authors

Sepideh Amjad-Iranagh − *Department of Materials and Metallurgical Engineering, Amirkabir University of Technology (Tehran Polytechnic), Tehran 15875-4313, Iran;* orcid.org/0000-0002-3220-7992; Email: amjad_i_s@aut.ac.ir

Rouein Halladj − *Department of Chemical Engineering, Amirkabir University of Technology (Tehran Polytechnic), Tehran 15875-4313, Iran;* orcid.org/0000-0001-9887-5435; Email: halladj@aut.ac.ir

Author

Atefeh Gholizadeh − *Department of Chemical Engineering, Amirkabir University of Technology (Tehran Polytechnic), Tehran 15875-4313, Iran*

Complete contact information is available at: https://pubs.acs.org/10.1021/acsomega.4c02551

Notes

The authors declare no competing financial interest.

ACKNOWLEDGMENTS

This research received no financial support from public, commercial, or nonprofit organizations.

REFERENCES

(1) Tsuruta, T.; Hayashi, T.; Kataoka, K.; Ishihara, K. *Biomedical Applications of Polymeric Materials*; CRC Press, 1993.

(2) Srinivas, G.; Mohan, R. V.; Kelkar, A. D. Polymer micelle assisted transport and delivery of model hydrophilic components inside a biological lipid vesicle: a coarse-grain simulation study. *J. Phys. Chem. B* **2013**, *117* (40), 12095−12104.

(3) Kordzadeh, A.; Amjad-Iranagh, S.; Zarif, M.; Modarress, H. Adsorption and encapsulation of the drug doxorubicin on covalent functionalized carbon nanotubes: A scrutinized study by using molecular dynamics simulation and quantum mechanics calculation. *J. Mol. Graphics Modell.* **2019**, *88*, 11−22.

(4) Zamani, F.; Jahanmard, F.; Ghasemkhah, F.; Amjad-Iranagh, S.; Bagherzadeh, R.; Amani-Tehran, M.; Latifi, M. Nanofibrous and Nanoparticle Materials as Drug-delivery Systems. In *Nanostructures for Drug Delivery*; Elsevier, 2017; pp 239−270.

(5) Gaucher, G.; Dufresne, M.-H.; Sant, V. P.; Kang, N.; Maysinger, D.; Leroux, J.-C. Block copolymer micelles: preparation, characterization and application in drug delivery. *J. Controlled Release* **2005**, *109* (1−3), 169−188.

(6) Aliabadi, H. M.; Lavasanifar, A. Polymeric micelles for drug delivery. *Expert Opin. Drug Delivery* **2006**, *3* (1), 139−162.

(7) Yang, J.; Wang, R.; Xie, D. Precisely controlled incorporation of drug nanoparticles in polymer vesicles by amphiphilic copolymer tethers. *Macromolecules* **2018**, *51* (17), 6810−6817.

(8) Rupar, P. A.; Chabanne, L.; Winnik, M. A.; Manners, I. Non-centrosymmetric cylindrical micelles by unidirectional growth. *Science* **2012**, *337*, 559−562.
(9) Hammouda, B. Temperature effect on the nanostructure of sds micelles in water. *J. Res. Natl. Inst. Stand. Technol.* **2013**, *118*, No. 151.
(10) Sugioka, H.; Matsuoka, K.; Moroi, Y. Temperature effect on formation of sodium cholate micelles. *J. Colloid Interface Sci.* **2003**, *259* (1), 156−162.
(11) Lindman, B.; Medronho, B.; Karlström, G. Clouding of nonionic surfactants. *Curr. Opin. Colloid Interface Sci.* **2016**, *22*, 23−29.
(12) Moulik, S. Micelles: self-organized surfactant assemblies. *Curr. Sci.* **1996**, 368−376.
(13) Yousefpour, A.; Amjad-Iranagh, S.; Goharpey, F.; Modarress, H. Effect of drug amlodipine on the charged lipid bilayer cell membranes dmps and dmps+ dmpc: A molecular dynamics simulation study. *Eur. Biophys. J.* **2018**, *47* (8), 939−950.
(14) Palladino, P.; Rossi, F.; Ragone, R. Effective critical micellar concentration of a zwitterionic detergent: a fluorimetric study on n-dodecyl phosphocholine. *J. Fluoresc.* **2010**, *20* (1), 191−196.
(15) Tieleman, D. P.; van der Spoel, D.; Berendsen, H. J. C. Molecular dynamics simulations of dodecylphosphocholine micelles at three different aggregate sizes: micellar structure and chain relaxation. *J. Phys. Chem. B* **2000**, *104* (27), 6380−6388.
(16) Gu, H.; Kato, T.; Kumeta, H.; Kumaki, Y.; Tsukamoto, T.; Kikukawa, T.; Demura, M.; Ishida, H.; Vogel, H. J.; Aizawa, T. Three-dimensional structure of the antimicrobial peptide cecropin p1 in dodecylphosphocholine micelles and the role of the c-terminal residues. *ACS Omega* **2022**, *7* (36), 31924−31934.
(17) Liu, D.-Z.; Lecluyse, E. L.; Thakker, D. R. Dodecylphosphocholine-mediated enhancement of paracellular permeability and cytotoxicity in caco-2 cell monolayers. *J. Pharm. Sci.* **1999**, *88* (11), 1161−1168.
(18) Rouse, S. L.; Marcoux, J.; Robinson, C. V.; Sansom, M. S. Dodecyl maltoside protects membrane proteins in vacuo. *Biophys. J.* **2013**, *105* (3), 648−656.
(19) Fei, Z.; Yoosefian, M. Design and development of polymeric micelles as nanocarriers for anti-cancer ribociclib drug. *J. Mol. Liq.* **2021**, *329*, No. 115574.
(20) Vincent, M.; Gallay, J.; Jamin, N.; Garrigos, M.; de Foresta, B. The predicted transmembrane fragment 17 of the human multidrug resistance protein 1 (mrp1) behaves as an interfacial helix in membrane mimics. *Biochim. Biophys. Acta, Biomembr.* **2007**, *1768* (3), 538−552.
(21) de Foresta, B.; Vincent, M.; Gallay, J.; Garrigos, M. Interaction with membrane mimics of transmembrane fragments 16 and 17 from the human multidrug resistance abc transporter 1 (hmrp1/abcc1) and two of their tryptophan variants. *Biochim. Biophys. Acta, Biomembr.* **2010**, *1798* (3), 401−414.
(22) Peterson, A. M.; Heemstra, J. M. Controlling self-assembly of dna-polymer conjugates for applications in imaging and drug delivery. *WIREs Nanomed. Nanobiotechnol.* **2015**, *7* (3), 282−297.
(23) Rabinowicz, A. L.; Carrazana, E.; Maggio, E. T. Improvement of intranasal drug delivery with intravail alkylsaccharide excipient as a mucosal absorption enhancer aiding in the treatment of conditions of the central nervous system. *Drugs R&D* **2021**, *21* (4), 361−369.
(24) Deuflhard, P.; Hermans, J.; Leimkuhler, B.; Mark, A. E.; Reich, S.; Skeel, R. D. *Computational Molecular Dynamics: Challenges, Methods, Ideas*; Springer Science & Business Media, 2012; Vol. *4*.
(25) Hinchliffe, A. *Molecular Modelling for Beginners*; John Wiley & Sons, 2003.
(26) Kavyani, S.; Amjad-Iranagh, S.; Dadvar, M.; Modarress, H. Hybrid dendrimers of ppi (core)-pamam (shell): A molecular dynamics simulation study. *J. Phys. Chem. B* **2016**, *120* (36), 9564−9575.
(27) Rahimi, A.; Amjad-Iranagh, S.; Modarress, H. Molecular dynamics simulation of coarse-grained poly (l-lysine) dendrimers. *J. Mol. Model.* **2016**, *22* (3), No. 59.
(28) Krüger, D. M.; Kamerlin, S. C. L. Micelle maker: An online tool for generating equilibrated micelles as direct input for molecular dynamics simulations. *ACS Omega* **2017**, *2* (8), 4524−4530.
(29) Chien, S.-C.; Pérez-Sánchez, G.; Gomes, J. R.; Cordeiro, M. N. D.; Jorge, M.; Auerbach, S. M.; Monson, P. A. Molecular simulations of the synthesis of periodic mesoporous silica phases at high surfactant concentrations. *J. Phys. Chem. C* **2017**, *121* (8), 4564−4575.
(30) Kavyani, S.; Dadvar, M.; Modarress, H.; Amjad-Iranagh, S. A coarse grained molecular dynamics simulation study on the structural properties of carbon nanotube-dendrimer composites. *Soft Matter* **2018**, *14* (16), 3151−3163.
(31) Monticelli, L.; Kandasamy, S. K.; Periole, X.; Larson, R. G.; Tieleman, D. P.; Marrink, S.-J. The martini coarse-grained force field: Extension to proteins. *J. Chem. Theory Comput.* **2008**, *4* (5), 819−834.
(32) Peroukidis, S. D.; Tsalikis, D. G.; Noro, M. G.; Stott, I. P.; Mavrantzas, V. G. Quantitative prediction of the structure and viscosity of aqueous micellar solutions of ionic surfactants: a combined approach based on coarse-grained martini simulations followed by reverse-mapped all-atom molecular dynamics simulations. *J. Chem. Theory Comput.* **2020**, *16* (5), 3363−3372.
(33) Subbalakshmi, C.; Sitaram, N. Mechanism of antimicrobial action of indolicidin. *FEMS Microbiol. Lett.* **1998**, *160* (1), 91−96.
(34) Robinson, W. E., Jr; McDougall, B.; Tran, D.; Selsted, M. E. Anti-hiv-1 activity of indolicidin, an antimicrobial peptide from neutrophils. *J. Leukocyte Biol.* **1998**, *63* (1), 94−100.
(35) Krajewski, K.; Marchand, C.; Long, Y.-Q.; Pommier, Y.; Roller, P. P. Synthesis and hiv-1 integrase inhibitory activity of dimeric and tetrameric analogs of indolicidin. *Bioorg. Med. Chem. Lett.* **2004**, *14* (22), 5595−5598.
(36) Hsu, C.-H.; Chen, C.; Jou, M.-L.; Lee, A. Y.-L.; Lin, Y.-C.; Yu, Y.-P.; Huang, W.-T.; Wu, S.-H. Structural and dna-binding studies on the bovine antimicrobial peptide, indolicidin: evidence for multiple conformations involved in binding to membranes and dna. *Nucleic Acids Res.* **2005**, *33* (13), 4053−4064.
(37) Friedrich, C. L.; Rozek, A.; Patrzykat, A.; Hancock, R. E. Structure and mechanism of action of an indolicidin peptide derivative with improved activity against gram-positive bacteria. *J. Biol. Chem.* **2001**, *276* (26), 24015−24022.
(38) Subbalakshmi, C.; Krishnakumari, V.; Nagaraj, R.; Sitaram, N. Requirements for antibacterial and hemolytic activities in the bovine neutrophil derived 13-residue peptide indolicidin. *FEBS Lett.* **1996**, *395* (1), 48−52.
(39) Halevy, R.; Rozek, A.; Kolusheva, S.; Hancock, R. E.; Jelinek, R. Membrane binding and permeation by indolicidin analogs studied by a biomimetic lipid/polydiacetylene vesicle assay. *Peptides* **2003**, *24* (11), 1753−1761.
(40) Rozek, A.; Friedrich, C. L.; Hancock, R. E. Structure of the bovine antimicrobial peptide indolicidin bound to dodecylphosphocholine and sodium dodecyl sulfate micelles. *Biochemistry* **2000**, *39* (51), 15765−15774.
(41) Yeh, I.-C.; Ripoll, D. R.; Wallqvist, A. Free energy difference in indolicidin attraction to eukaryotic and prokaryotic model cell membranes. *J. Phys. Chem. B* **2012**, *116* (10), 3387−3396.
(42) Hakobyan, D.; Heuer, A. Phase separation in a lipid/cholesterol system: comparison of coarse-grained and united-atom simulations. *J. Phys. Chem. B* **2013**, *117* (14), 3841−3851.
(43) Choubey, A.; Kalia, R. K.; Malmstadt, N.; Nakano, A.; Vashishta, P. Cholesterol translocation in a phospholipid membrane. *Biophys. J.* **2013**, *104* (11), 2429−2436.
(44) Yesylevskyy, S. O.; Demchenko, A. P. Cholesterol Behavior in Asymmetric Lipid Bilayers: Insights from Molecular Dynamics Simulations. In *Methods in Membrane Lipids*; Springer, 2015; pp 291−306.
(45) Bemporad, D.; Luttmann, C.; Essex, J. Computer simulation of small molecule permeation across a lipid bilayer: dependence on bilayer properties and solute volume, size, and cross-sectional area. *Biophys. J.* **2004**, *87* (1), 1−13.

https://doi.org/10.1021/acsomega.4c02551
ACS Omega 2024, 9, 40433−40445

(46) Kopeć, W.; Telenius, J.; Khandelia, H. Molecular dynamics simulations of the interactions of medicinal plant extracts and drugs with lipid bilayer membranes. *FEBS J.* **2013**, *280* (12), 2785−2805.
(47) Amjad-Iranagh, S.; Yousefpour, A.; Haghighi, P.; Modarress, H. Effects of protein binding on a lipid bilayer containing local anesthetic articaine, and the potential of mean force calculation: a molecular dynamics simulation approach. *J. Mol. Model.* **2013**, *19* (9), 3831−3842.
(48) Nademi, Y.; Iranagh, S. A.; Yousefpour, A.; Mousavi, S. Z.; Modarress, H. Molecular dynamics simulations and free energy profile of paracetamol in dppc and dmpc lipid bilayers. *J. Chem. Sci.* **2014**, *126* (3), 637−647.
(49) Yousefpour, A.; Iranagh, S. A.; Nademi, Y.; Modarress, H. Molecular dynamics simulation of nonsteroidal antiinflammatory drugs, naproxen and relafen, in a lipid bilayer membrane. *Int. J. Quantum Chem.* **2013**, *113* (15), 1919−1930.
(50) Sankaram, M. B.; Thompson, T. E. Interaction of cholesterol with various glycerophospholipids and sphingomyelin. *Biochemistry* **1990**, *29* (47), 10670−10675.
(51) Zhuang, X.; Makover, J. R.; Im, W.; Klauda, J. B. A systematic molecular dynamics simulation study of temperature dependent bilayer structural properties. *Biochim. Biophys. Acta, Biomembr.* **2014**, *1838* (10), 2520−2529.
(52) Theng, S. G.; Jumbri, K.; Wirzal, M. D. H. In *Molecular Dynamics Simulation of Membrane in Room Temperature Ionic Liquids*, AIP Conference Proceedings; AIP Publishing LLC, 2017020133.
(53) Van Der Spoel, D.; Lindahl, E.; Hess, B.; Groenhof, G.; Mark, A. E.; Berendsen, H. J. Gromacs: fast, flexible, and free. *J. Comput. Chem.* **2005**, *26* (16), 1701−1718.
(54) Abraham, M.; Van Der Spoel, D.; Lindahl, E.; Hess, B. the gromacs development team, gromacs user manual version 2018. 2018.
(55) Yesylevskyy, S. O.; Schäfer, L. V.; Sengupta, D.; Marrink, S. J. Polarizable water model for the coarse-grained martini force field. *PLoS Comput. Biol.* **2010**, *6* (6), No. e1000810.
(56) Marrink, S. J.; De Vries, A. H.; Mark, A. E. Coarse grained model for semiquantitative lipid simulations. *J. Phys. Chem. B* **2004**, *108* (2), 750−760.
(57) Wassenaar, T. A.; Ingólfsson, H. I.; Bckmann, R. A.; Tieleman, D. P.; Marrink, S. J. Computational lipidomics with insane: a versatile tool for generating custom membranes for molecular simulations. *J. Chem. Theory Comput.* **2015**, *11* (5), 2144−2155.
(58) Martínez, L.; Andrade, R.; Birgin, E. G.; Martinez, J. M. Packmol: a package for building initial configurations for molecular dynamics simulations. *J. Comput. Chem.* **2009**, *30* (13), 2157−2164.
(59) Zhang, L.; Somasundaran, P.; Maltesh, C. Electrolyte effects on the surface tension and micellization of n-dodecyl β-d-maltoside solutions. *Langmuir* **1996**, *12* (10), 2371−2373.
(60) Curry, H. B. The method of steepest descent for non-linear minimization problems. *Q. Appl. Math.* **1944**, *2* (3), 258−261.
(61) Bussi, G.; Donadio, D.; Parrinello, M. Canonical sampling through velocity rescaling. *J. Chem. Phys.* **2007**, *126* (1), No. 014101.
(62) Berendsen, H. J. C.; Postma, J. P. M.; van Gunsteren, W. F.; Hermans, J. Interaction Models for Water in Relation to Protein Hydration. In *The Jerusalem Symposia on Quantum Chemistry and Biochemistry*; Springer, 1981; pp 331−342.
(63) Rahman, A.; Stillinger, F. H. Molecular dynamics study of liquid water. *J. Chem. Phys.* **1971**, *55* (7), 3336−3359.
(64) Parrinello, M.; Rahman, A. Polymorphic transitions in single crystals: A new molecular dynamics method. *J. Appl. Phys.* **1981**, *52* (12), 7182−7190.
(65) Winger, M.; Trzesniak, D.; Baron, R.; van Gunsteren, W. F. On using a too large integration time step in molecular dynamics simulations of coarse-grained molecular models. *Phys. Chem. Chem. Phys.* **2009**, *11*, 1934−1941.
(66) Marrink, S. J.; Periole, X.; Tieleman, D. P.; de Vries, A. H. Comment on "on using a too large integration time step in molecular dynamics simulations of coarse-grained molecular models" by m. winger, d. trzesniak, r. baron and wf van gunsteren, phys. chem. chem. phys., 2009, 11, 1934. *Phys. Chem. Chem. Phys.* **2010**, *12* (9), 2254−2256.
(67) de Jong, D. H.; Singh, G.; Bennett, W. D.; Arnarez, C.; Wassenaar, T. A.; Schafer, L. V.; Periole, X.; Tieleman, D. P.; Marrink, S. J. Improved parameters for the martini coarse-grained protein force field. *J. Chem. Theory Comput.* **2013**, *9* (1), 687−697.
(68) Humphrey, W.; Dalke, A.; Schulten, K. Vmd: visual molecular dynamics. *J. Mol. Graphics* **1996**, *14* (1), 33−38.
(69) Redondo-Morata, L.; Giannotti, M. I.; Sanz, F. Influence of cholesterol on the phase transition of lipid bilayers: A temperature-controlled force spectroscopy study. *Langmuir* **2012**, *28* (35), 12851−12860.
(70) Torrie, G. M.; Valleau, J. P. Nonphysical sampling distributions in monte carlo free-energy estimation: Umbrella sampling. *J. Comput. Phys.* **1977**, *23* (2), 187−199.
(71) Mousavi, S. Z.; Amjad-Iranagh, S.; Nademi, Y.; Modarress, H. Carbon nanotube-encapsulated drug penetration through the cell membrane: an investigation based on steered molecular dynamics simulation. *J. Membr. Biol.* **2013**, *246* (9), 697−704.
(72) Yousefpour, A.; Modarress, H.; Goharpey, F.; Amjad-Iranagh, S. Interaction of pegylated anti-hypertensive drugs, amlodipine, atenolol and lisinopril with lipid bilayer membrane: a molecular dynamics simulation study. *Biochim. Biophys. Acta, Biomembr.* **2015**, *1848* (8), 1687−1698.
(73) Berendsen, H. J. C.; Postma, J. P. M.; van Gunsteren, W. F.; DiNola, A.; Haak, J. R. Molecular dynamics with coupling to an external bath. *J. Chem. Phys.* **1984**, *81* (10), 3684−3690.
(74) Milner, S. T. Chain architecture and asymmetry in copolymer microphases. *Macromolecules* **1994**, *27* (8), 2333−2335.
(75) Lee, B.; Richards, F. M. The interpretation of protein structures: estimation of static accessibility. *J. Mol. Biol.* **1971**, *55* (3), No. 379-IN4.
(76) Smith, J. M. "Introduction to chemical engineering thermodynamics", 1950.
(77) Eisenberg, D.; McLachlan, A. D. Solvation energy in protein folding and binding. *Nature* **1986**, *319*, 199−203.
(78) Hofsäß, C.; Lindahl, E.; Edholm, O. Molecular dynamics simulations of phospholipid bilayers with cholesterol. *Biophys. J.* **2003**, *84* (4), 2192−2206.
(79) Lyubartsev, A. P.; Laaksonen, A. Concentration effects in aqueous nacl solutions. a molecular dynamics simulation. *J. Phys. Chem. A* **1996**, *100* (40), 16410−16418.
(80) Khajeh, A.; Modarress, H. Effect of cholesterol on behavior of 5-fluorouracil (5-fu) in a dmpc lipid bilayer, a molecular dynamics study. *Biophys. Chem.* **2014**, *187*−*188*, 43−50.
(81) Abel, S.; Dupradeau, F.-Y.; Marchi, M. Molecular dynamics simulations of a characteristic dpc micelle in water. *J. Chem. Theory Comput.* **2012**, *8* (11), 4610−4623.
(82) Abel, S.; Dupradeau, F.-Y.; Raman, E. P.; MacKerell, A. D., Jr; Marchi, M. Molecular simulations of dodecyl-β-maltoside micelles in water: influence of the headgroup conformation and force field parameters. *J. Phys. Chem. B* **2011**, *115* (3), 487−499.
(83) Wu, W.; Zou, Z.; Yang, S.; Wu, Q.; Li, W.; Ding, Q.; Guan, Z.; Zhu, W. Coarse-grained molecular dynamic and experimental studies on self-assembly behavior of nonionic f127/hs15 mixed micellar systems. *Langmuir* **2020**, *36* (8), 2082−2092.
(84) Moradi, S.; Taran, M.; Mohajeri, P.; Sadrjavadi, K.; Sarrami, F.; Karton, A.; Shahlaei, M. Study of dual encapsulation possibility of hydrophobic and hydrophilic drugs into a nanocarrier based on biopolymer coated graphene oxide using density functional theory, molecular dynamics simulation and experimental methods. *J. Mol. Liq.* **2018**, *262*, 204−217.
(85) Tanford, C. Thermodynamics of micelle formation: prediction of micelle size and size distribution. *Proc. Natl. Acad. Sci. U.S.A.* **1974**, *71* (5), 1811−1815.
(86) Abel, S.; Lorieau, A.; de Foresta, B.; Dupradeau, F.-Y.; Marchi, M. Bindings of hmrp1 transmembrane peptides with dodecylphosphocholine and dodecyl-β-d-maltoside micelles: A molecular

https://doi.org/10.1021/acsomega.4c02551
ACS Omega 2024, 9, 40433−40445

dynamics simulation study. *Biochim. Biophys. Acta, Biomembr.* **2014**, *1838* (1), 493−509.
(87) Nagle, J. Area/lipid of bilayers from nmr. *Biophys. J.* **1993**, *64* (5), 1476−1481.
(88) Wang, Y.; Gkeka, P.; Fuchs, J. E.; Liedl, K. R.; Cournia, Z. Dppc-cholesterol phase diagram using coarse-grained molecular dynamics simulations. *Biochim. Biophys. Acta, Biomembr.* **2016**, *1858* (11), 2846−2857.
(89) Xiang, T.-X.; Anderson, B. D. Liposomal drug transport: a molecular perspective from molecular dynamics simulations in lipid bilayers. *Adv. Drug Delivery Rev.* **2006**, *58* (12−13), 1357−1378.
(90) Salassi, S.; Simonelli, F.; Bartocci, A.; Rossi, G. A martini coarse-grained model of the calcein fluorescent dye. *J. Phys. D: Appl. Phys.* **2018**, *51* (38), No. 384002.
(91) Boggara, M. B.; Krishnamoorti, R. Partitioning of nonsteroidal antiinflammatory drugs in lipid membranes: a molecular dynamics simulation study. *Biophys. J.* **2010**, *98* (4), 586−595.

https://doi.org/10.1021/acsomega.4c02551
ACS Omega 2024, 9, 40433−40445